MJFAS
Malaysian Journal of Fundamental and Applied Sciences

Najjar *et al.* | Malaysian Journal of Fundamental and Applied Sciences, Vol. 19 (2023) 389-398

RESEARCH ARTICLE

# Classification of COVID-19 from X-ray Images using GLCM Features and Machine Learning

**Fallah H Najjar [a,c,*], Karrar A Kadhim[b,c], Munaf Hamza Kareem[a], Hanan Abbas Salman[a], Duha Amer Mahdi[a], Horya M Al-Hindawi[d]**

[a]Department of Computer System Techniques, Technical Institute of Najaf, Al-Furat Al-Awsat Technical University, Iraq; [b]Computer Techniques Engineering Department, Faculty of Information Technology, Imam Jaafar Al-Sadiq University, Baghdad, Iraq; [c]Faculty of Engineering, School of Computing, Universiti Teknologi Malaysia, 81310 UTM Johor Bahru, Johor, Malaysia; [d]Computer Engineering Department, Faculty of Engineering, Mustansiriyah University, Baghdad, Iraq

Abstract As the world continues to battle the devastating effects of the COVID-19 pandemic, it has become increasingly crucial to screen patients for contamination accurately and effectively. One of the primary screening methods is chest radiography, utilizing radiological imaging to detect the presence of the virus in the lungs. This study presents a cutting-edge solution to classify COVID-19 infections in chest X-ray images by utilizing the Gray-Level Co-occurrence Matrix (GLCM) and machine learning algorithms. The proposed method analyzes each X-ray image using the GLCM to extract 22 statistical texture features and then trains two machine learning classifiers - K-Nearest Neighbor and Support Vector Machine - on these features. The method was tested on the COVID-19 Radiography Database and was compared to a state-of-the-art method, delivering highly efficient results with impressive sensitivity, accuracy, precision, F1-score, specificity, and Matthew's correlation coefficient. The proposed approach offers a promising new way to classify COVID-19 infections in chest X-ray images and has the potential to play a crucial role in the ongoing fight against the pandemic.

**Keywords**: COVID-19, feature extraction, GLCM, kNN, SVM.

## Introduction

***For correspondence:**
fallahnajjar@atu.edu.iq

**Received:** 5 Nov. 2022
**Accepted:** 11 April 2023



The sudden spread of COVID-19 rocked the world, and the World Health Organization (WHO) declared a pandemic on 11 March 2020 due to its contagious nature [1]. The severity of the virus prompted deep concerns about its alarming transmission rate. SARS-CoV2, the culprit behind Severe Acute Respiratory Syndrome, earned its name [2-4]. The virus first surfaced in China and quickly spread to other nations, becoming a worldwide pandemic within a few years [5]. Despite the tireless efforts of medical professionals, the virus continues to claim lives, hindered by its recent emergence, late detection, and striking resemblance to pneumonia [6,7]. COVID-19 detection relies on radiological imaging techniques, with X-ray scans showing their early and late stages. However, its circular appearance in scans can resemble other viral lung diseases, making it challenging to distinguish from healthy individuals. This paper introduces the Gray-Level Co-occurrence Matrix (GLCM) with 22 features and machine learning classifiers to classify COVID-19 infections in chest X-ray images, overcoming the difficulties of differentiation.

Artificial Intelligence has a subfield, Machine Learning that plays a crucial role in the medical field, particularly in extracting features and analyzing images. For example, with its help, various medical

10.11113/mjfas.v19n3.2911

images, like X-rays, tumor diagnoses, and cystoscopic images of viral pneumonia, can be analyzed and studied.

For example, the X-ray images of COVID-19 tend to have a unique shading and distribution, which can be recognized with ML techniques. To classify COVID-19 X-ray images, various ML and feature extraction methods have been proposed, with the GLCM [5] being a standout among them for its ability to produce valuable and meaningful features for fast and successful classification [8].

Typically, GLCM is known for its ability to extract robust statistical texture features, with many researchers utilizing it as a secondary feature extraction method, in addition to other techniques, in the MATLAB image processing toolbox, where only four features (contrast, correlation, energy, and inverse difference moment/homogeneity) [9-13] are extracted. This paper, however, introduces a set of 22 features extracted from the GLCM matrices, going beyond the standard four features to include Contrast, Angular Second Moment, Inverse Difference Moment/Local Homogeneity, Entropy, Maximum Joint Probability, Joint Average, Joint Variance, Dissimilarity, Normalized Inverse Difference Moment, Correlation, Autocorrelation, Difference Average, Difference Variance, Difference Entropy, Energy, Cluster Prominence, Cluster Shade, Inertia, Cluster Tendency, Maximum Correlation Coefficient, Information Measure of Correlation (1), and Information Measure of Correlation (2). However, GLCM is usually used as a secondary feature extractor method [14, 15].

## Related Works

The COVID-19 pandemic has left a devastating impact on the world, causing widespread chaos in various industries. In response, machine learning and medical image analysis researchers have been working tirelessly to develop high-performance COVID-19 image analysis systems. Feature extraction methods have been integral to this effort, allowing researchers to uncover crucial information from medical and COVID-19 X-Ray images.

Studies in this field have produced a wealth of information on the topic, including GLCM feature extraction. In [16], a method was proposed that used GLCM to extract features from the image dataset with three distances and directions. However, this was then classified with the Dense fully connected and SoftMax layer. In [9], GLCM was used as a secondary feature extraction method, extracting only four features (equations 2, 4, 11, and 16).

Another study [14] combined the GLCM method with six other methods, resulting in the extraction of 1308 features, including 56 from GLCM. The method employed the Principal Component Analysis (PCA) to reduce the number of extracted features and the adaptive histogram equalization algorithm to enhance image contrast. This study took a minimalistic approach, with no enhancement, preprocessing, noise reduction, feature reduction, or image improvement operations utilized.

Shaban *et al*. [17] used a more traditional machine learning approach, incorporating GLCM features optimized by the Hybrid FS model (HFSM) and classified using the Enhanced KNN (EKNN) classifier. Despite this, the proposed CGRO algorithm still managed to outperform its competition in terms of classification results.

In conclusion, GLCM has proven to be a valuable tool in the quest for high-performance COVID-19 image analysis systems, offering researchers a robust method for extracting crucial information from medical and X-Ray images.

## Methodology

The COVID-19 dataset is created using images from the COVID-19 Radiography Database chest X-Ray images. COVID-19 Radiography Database contains 33,920 chest X-ray images. Therefore, we randomly take only 2399 chest X-ray images: 1577 NORMAL and 822 COVID-19 from the COVID-19 Radiography Database. These images are stored as gray-scale images having a size of 299x299. Samples of the input images are shown in Figure 1.

Initially, the input image is resized to 512x512 and divided into four quarters. Hence, there is no image denoising or enhancement on the input image. The proposed method extracts twenty-two features from the GLCM matrices using equations (2 - 20 and 22 - 24).

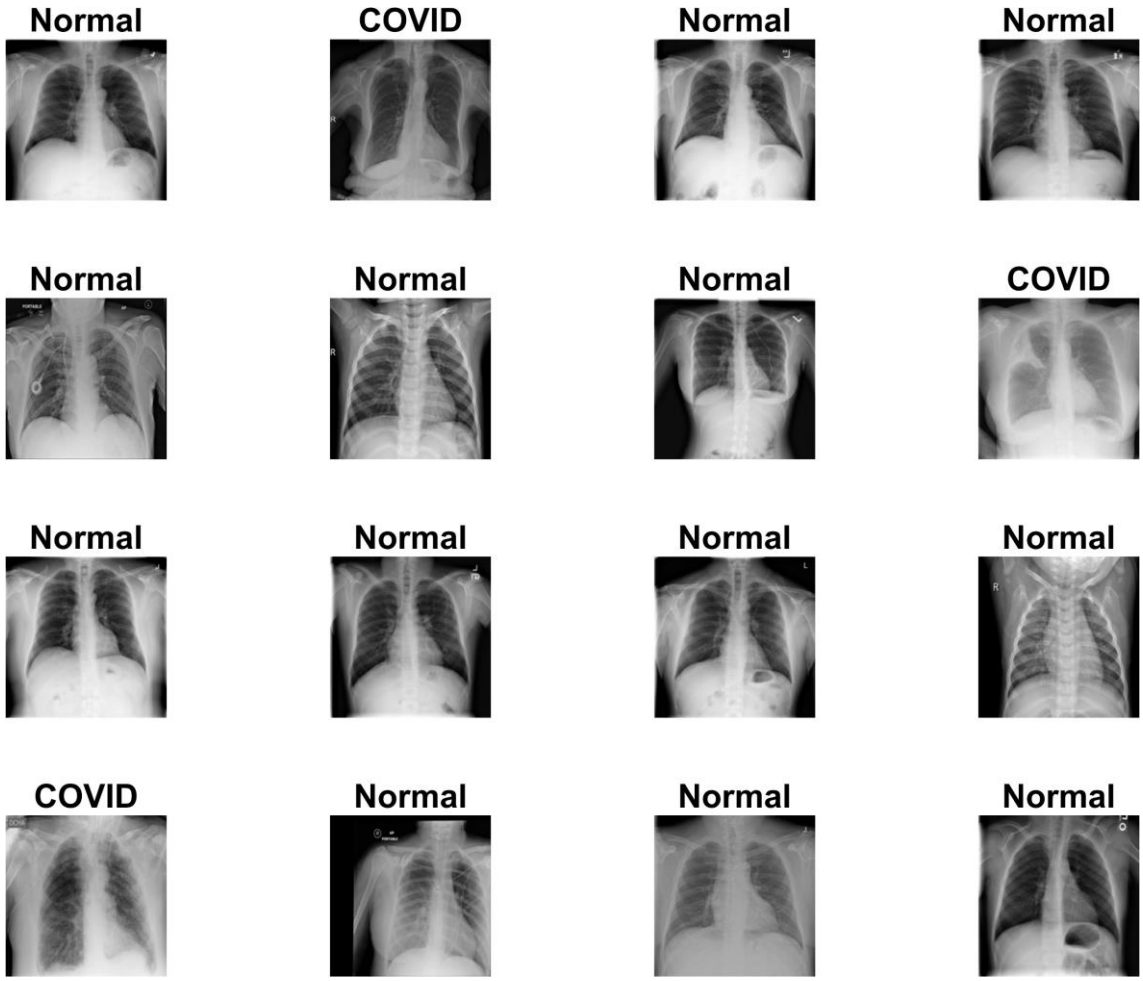


**Figure 1.** Samples of Normal and COVID-19 chest X-Ray images

Then, the proposed method produces five matrices (GLCM1, GLCM2, GLCM3, GLCM4, and GLCMA), each with 9596 rows, 22 features, and one target class. After that, the produced datasets are combined into one (COVID GLCM), containing 47980 rows, 22 attributes, and one target class. The purpose of the combination is to compare the proposed method with the state-of-the-art algorithms in the literature. Finally, all datasets are split into 80% for training and 20% for testing. In order to evaluate the proposed method, the GLCM1, GLCM2, GLCM3, GLCM4, and GLCMA datasets are classified utilizing two ML classifiers, namely, K-Nearest Neighbor (KNN) and Support Vector Machine (SVM), while the COVID GLCM dataset is also classified utilizing the KNN and SVM classifiers. The proposed method flow diagram is shown in Figure 2.

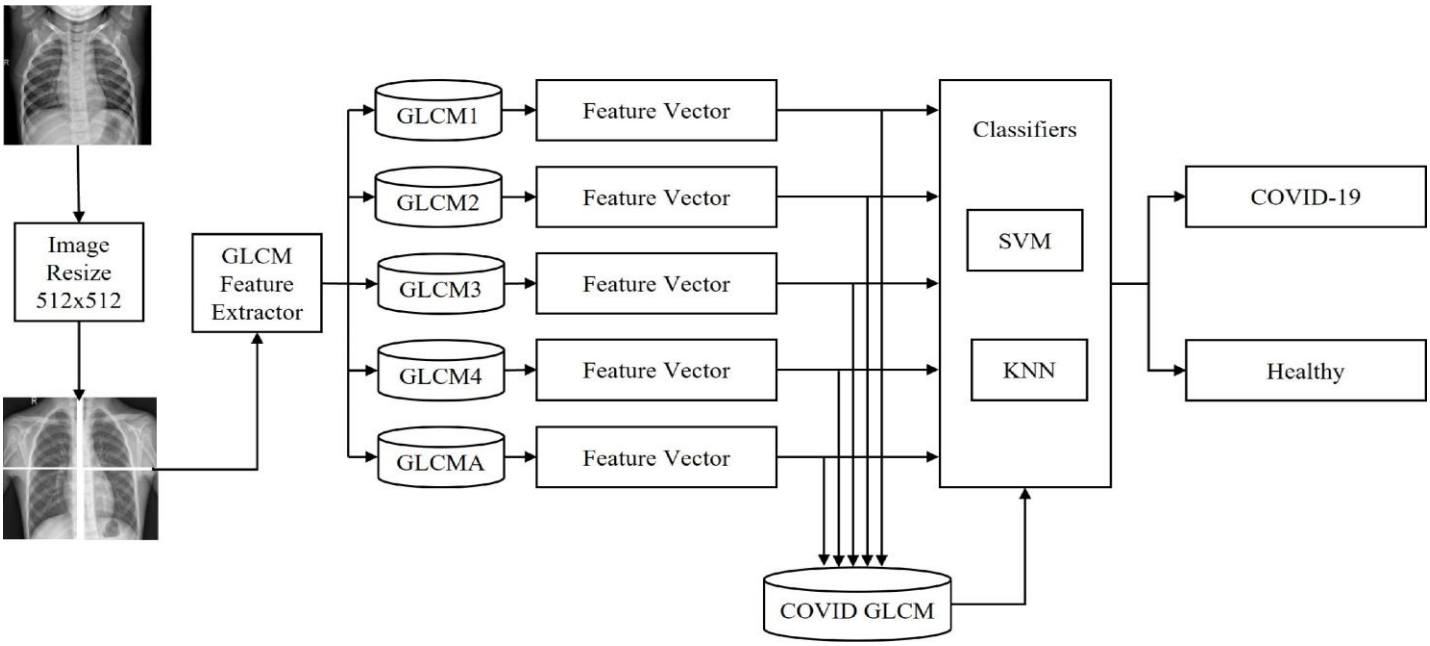


**Figure 2.** Flow diagram of the proposed method

## GLCM

The GLCM is a statistical method to extract texture features from a matrix produced by calculating transitions between pairs of two pixels. This matrix with the size is equal to the maximum value of the original matrix or image. The GLCM technique was familiarized by Haralick [5], which used it for image classification by extracting features from GLCM. It depends on two main parameters; one is d, called distance, and the other is angular θ. For example, where d is the distance between two pixels and θ is the direction must go, it may be equal to 0, 45, 90, and 135. Therefore, GLCM can be defined as the following equation:

$$p(r,c|d,\theta) = \frac{N_{d,\theta}(r,c)}{N}$$

Where N: represents the summation of all transitions.

However, now is an example to explain how GLCM works: First, let the matrix in Figure 5 is the original matrix, d=1, and θ=0. So.

| | | | |
|---|---|---|---|
| 1 | 1 | 0 | 2 |
| 0 | 0 | 3 | 3 |
| 2 | 2 | 1 | 1 |
| 2 | 1 | 0 | 1 |

**Figure 3.** Original matrix (G)

Next, a matrix with max(G)×max(G) is created. Here, the max value in matrix G is 3. See Figure 4

| | 0 | 1 | 2 | 3 |
|---|---|---|---|---|
| 0 | 0, 0 | 0, 1 | 0, 2 | 0, 3 |
| 1 | 1, 0 | 1, 1 | 1, 2 | 1, 3 |
| 2 | 2, 0 | 2, 1 | 2, 2 | 2, 3 |
| 3 | 3, 0 | 3, 1 | 3, 2 | 3, 3 |

**Figure 4.** Matrix representation (A)

The value of the first location in matrix A(1,1) calculating by counting how many pixels with value 1 in the original matrix have neighbors with value (1) on the left and right with distance (1) equal to d. Also, the location $A(1,2)$ is the counting of pixels with value (1), and its neighbor has value (2) on the left and right. And so on for all locations and all angular; see Figure 5.

| | 0 | 1 | 2 | 3 |
|---|---|---|---|---|
| 0 | 2 | 3 | 1 | 1 |
| 1 | 3 | 4 | 2 | 0 |
| 2 | 1 | 2 | 2 | 0 |
| 3 | 1 | 0 | 0 | 2 |

$\theta = 0$

| | 0 | 1 | 2 | 3 |
|---|---|---|---|---|
| 0 | 2 | 2 | 1 | 0 |
| 1 | 2 | 2 | 0 | 1 |
| 2 | 1 | 0 | 2 | 2 |
| 3 | 0 | 1 | 2 | 0 |

$\theta = 45$

| | 0 | 1 | 2 | 3 |
|---|---|---|---|---|
| 0 | 0 | 3 | 2 | 1 |
| 1 | 3 | 2 | 1 | 2 |
| 2 | 2 | 1 | 2 | 1 |
| 3 | 1 | 2 | 1 | 0 |

$\theta = 90$

| | 0 | 1 | 2 | 3 |
|---|---|---|---|---|
| 0 | 0 | 2 | 2 | 1 |
| 1 | 2 | 2 | 1 | 2 |
| 2 | 2 | 1 | 0 | 0 |
| 3 | 1 | 2 | 0 | 0 |

$\theta = 135$

**Figure 5.** GLCM with different θ, where θ=0,45,90, and 135, respectively

In the last step, the twenty-two texture features of the GLCM matrices we used to perform the proposed method are defined in Table 1 [10, 18, 19].

**Table 1.** Proposed extracted features

| Features | Equation | # |
|---|---|---|
| Contrast | $F_{Contrast} = \sum_{r=0}^{n-1}\sum_{c=0}^{m-1}(r-c)^2 \times im(r,c)$ | 2 |
| Angular Second Moment (ASM) | $F_{\mathrm{ASM}} = \sum_{r=0}^{n-1}\sum_{c=0}^{m-1} im(r,c)^2$ | 3 |
| Inverse Difference Moment (IDM) / Local Homogeneity | $F_{IDM} = \sum_{r=0}^{n-1}\sum_{c=0}^{m-1}\frac{1}{1+(r-c)^2} im(r,c)$ | 4 |
| Entropy | $F_{Entropy} = \sum_{r=0}^{n-1}\sum_{c=0}^{m-1} im(r,c) \times \log(im(r,c))$ | 5 |
| Joint Maximum probability (JM) | $F_{JM} = \sum_{r=0}^{n-1}\sum_{c=0}^{m-1}\max(im(r,c))$ | 6 |
| Joint Average (JA) | $F_{JA} = \sum_{r=0}^{n-1}\sum_{c=0}^{m-1} r\, im(r,c)$ | 7 |
| Joint Variance (JV) | $F_{JV} = \sum_{r=0}^{n-1}\sum_{c=0}^{m-1}(r-\mu_c)^2\, im(r,c)$ | 8 |
| Dissimilarity | $F_{Diss} = \sum_{r=0}^{n-1}\sum_{c=0}^{m-1}\lvert r-c\rvert\, im(r,c)$ | 9 |
| Normalized Inverse Difference Moment (NIDM) | $F_{NIDM} = \sum_{r=0}^{n-1}\sum_{c=0}^{m-1}\frac{1}{1+\lvert r-c\rvert/N_g} im(r,c)$ | 10 |

| Features | Equation | # |
|---|---|---|
| Correlation | $F_{Corr} = \frac{1}{\sigma_r^2} \sum_{r=0}^{n-1} \sum_{c=0}^{m-1} (r - \mu_r.)(c - \mu_r.)\ im(r,c)$ | 11 |
| Autocorrelation | $F_{AutoCorr} = \sum_{r=0}^{n-1} \sum_{c=0}^{m-1} r\ c\ im(r,c)$ | 12 |
| Difference Average (DA) | $F_{DA} = \sum_k k\ im(r,c)\,,k$ | 13 |
| Difference Variance (DV) | $F_{DV} = \sum_k (k - \mu)^2\ im(r,c)\,,k$ | 14 |
| Difference Entropy (DE) | $F_{DE} = \sum_k im(r,c)\,,k\ log_2 im(r,c),k$ | 15 |
| Energy | $F_{Energy} = \sqrt{\sum_{r=0}^{n-1} \sum_{c=0}^{m-1} im(r,c)^2}$ | 16 |
| Cluster Prominence (CP) | $F_{\mathrm{CP}} = \sum_{r=0}^{n-1} \sum_{c=0}^{m-1} \left\{r - c - \mu_{p_x}\mu_{p_y}\right\}^4 im(r,c)$ | 17 |
| Cluster Shade (CS) | $F_{\mathrm{CS}} = \sum_{r=0}^{n-1} \sum_{c=0}^{m-1} \left\{r - c - \mu_{p_x}\mu_{p_y}\right\}^3 im(r,c)$ | 18 |
| Inertia (In) | $F_{In} = \sum_{r=0}^{n-1} \sum_{c=0}^{m-1} (r - c)^2\ im(r,c)$ | 19 |
| Cluster Tendency (CT) | $F_{CT} = \sum_{r=0}^{n-1} \sum_{c=0}^{m-1} (r + c - \mu_{p_x} - \mu_{p_y})^2\ im(r,c)$ | 20 |
| Maximum Correlation Coefficient (MCC) | $F_{MCC} = (Second\ largest\ eigenvalue\ of\ Q)^{\frac{1}{2}}$ <br> Where $Q = \sum_{k=1}^{L} \frac{p(r,k)p(c,k)}{P_x(r)P_y(k)}$ | 22 |
| Information Measure Of Correlation 1 (IMC1) | $F_{\mathrm{MIC1}} = \frac{-\sum_{r=0}^{n-1}\sum_{c=0}^{m-1} p_{r,c}\ log_2(p_{r,c}) + \sum_{r=0}^{n-1}\sum_{c=0}^{m-1} p_{r,c}\ log_2(p_r,p_c)}{\sum_r p_r\ log_2\ p_r}$ | 23 |
| Information Measure Of Correlation 2 (MIC2) | $F_{\mathrm{MIC2}} = \sqrt{1 - \exp\left[-2 \sum_{r=0}^{n-1} \sum_{c=0}^{m-1} p_r\ p_c log_2(p_r,p_c) - \sum_{r=0}^{n-1} \sum_{c=0}^{m-1} p_{r,c}\ log_2(p_{r,c})\right]}$ | 24 |

## Classification Performance Metrics

The classification model assigns a predicted label (positive or negative) to each sample in order to predict the class in which the data will fall: It is thus possible to conclude that each sample falls into one of these categories: (1) Actual positives that are wrongly predicted negatives: False Negatives (FN), (2) Actual positives that are correctly predicted positives: True Positives (TP), (3) Actual negatives that are wrongly predicted positives: False Positives (FP), and (4) Actual negatives that are correctly predicted negatives: True Negatives (TN) [21-23].

The Confusion Matrix (CM), a two-by-two table, can be used to display this partition.

$$CM = \begin{bmatrix} TP & FN \\ FP & TN \end{bmatrix}$$

Usually, many metrics are based on the CM used to evaluate the performance of the ML classifier. In this paper, we used a number of these metrics, such as Matthews Correlation Coefficient (MCC), Sensitivity (SEN), F-Score (F1), Precision (PRE), Accuracy (ACC), and Specificity (SP). These evaluation metrics are defined in the following equations [20]:

$$SP = \frac{\mathrm{TN}}{(\mathrm{TN} + \mathrm{FP})} \quad (25)$$

$$ACC = \frac{(\mathrm{TP} + \mathrm{TN})}{(\mathrm{TP} + \mathrm{TN} + \mathrm{FN} + \mathrm{FP})} \quad (26)$$

$$SEN = \frac{\mathrm{TP}}{(\mathrm{TP} + \mathrm{FN})} \quad (27)$$

$$PRE = \frac{\mathrm{TP}}{(\mathrm{TP} + \mathrm{FP})} \quad (28)$$

$$F1 = 2 \times \frac{(\mathrm{PRE} \times \mathrm{SEN})}{(\mathrm{PRE} + \mathrm{SEN})} \quad (29)$$

$$MCC = \frac{(\mathrm{TP} \times \mathrm{TN}) - (\mathrm{FP} \times \mathrm{FN})}{\sqrt{(\mathrm{TP} + \mathrm{FP})(\mathrm{TN} + \mathrm{FN})(\mathrm{TP} + \mathrm{FN})(\mathrm{TN} + \mathrm{FP})}} \quad (30)$$

## Experimental Results

The proposed method is established on a PC with Intel Core i7-11800H (2.30 GHz, 16 CPU), 16 GB DDR4 RAM, and NVIDIA GeForce RTX 3050 TI GPU. MATLAB (R2022a) Image Processing toolbox was used for the coding. As already mentioned, the dataset contains 2399 chest X-ray images and consists of two classes. The COVID-19 class contains 822 images, while the NORMAL class contains 1577 images [24-27]. However, we used the proposed method to evaluate ACC, MCC, SEN, F1, PRE, and SP metrics (equations 25-32).

In this experiment, we calculate the evaluation metrics of the SVM and the KNN classifiers for the GLCM1, GLCM2, GLCM3, GLCM4, and GLCMA datasets. Table 2 and Table 3 demonstrate the ACC, F1, SEN, SP, PRE, and MCC results for SVM and KNN classifiers, respectively.

**Table 2.** SVM - Classification report for the proposed method

| Dataset | ACC | F1 | SEN | SP | PRE | MCC |
|---|---|---|---|---|---|---|
| GLCM1 | 0.9583 | 0.9685 | 0.9610 | 0.9530 | 0.9762 | 0.9071 |
| GLCM2 | 0.9521 | 0.9641 | 0.9486 | 0.9594 | 0.9802 | 0.8931 |
| GLCM3 | 0.9552 | 0.9663 | 0.9551 | 0.9554 | 0.9778 | 0.9000 |
| GLCM4 | 0.9557 | 0.9665 | 0.9608 | 0.9456 | 0.9722 | 0.9013 |
| GLCMA | 0.9594 | 0.9695 | 0.9554 | 0.9677 | 0.9841 | 0.9094 |

**Table 3.** KNN - Classification report for the proposed method

| Dataset | ACC | F1 | SEN | SP | PRE | MCC |
|---|---|---|---|---|---|---|
| GLCM1 | 0.9708 | 0.9782 | 0.9589 | 0.9967 | 0.9984 | 0.9358 |
| GLCM2 | 0.9703 | 0.9778 | 0.9595 | 0.9934 | 0.9968 | 0.9344 |
| GLCM3 | 0.9687 | 0.9767 | 0.9553 | 0.9983 | 0.9992 | 0.9313 |
| GLCM4 | 0.9724 | 0.9794 | 0.9597 | 1.0000 | 1.0000 | 0.9393 |
| GLCMA | 0.9687 | 0.9767 | 0.9580 | 0.9918 | 0.9960 | 0.9309 |

Furthermore, this subsection compares the proposed method with state-of-the-art algorithms [28-33]. Furthermore, the experimental results of the proposed method are collected on the COVID GLCM dataset using SVM and KNN classifiers. Compared to the other methods, the proposed method results were better concerning PRE, ACC, SEN, SP, F1, and MCC, as shown in Table 4.

**Table 4.** Our proposed method results compared with the state-of-art approaches

| Class | #Features | Classifiers | PRE | ACC | SEN | SP | F1 | MCC |
|---|---|---|---|---|---|---|---|---|
| Goyal *et al*. [7] | 64 | KNN | 0.7861 | 0.8154 | 0.8764 | 0.7672 | 0.8267 | - |
| Goyal *et al*. [7] | 64 | SVM | 0.7722 | 0.8194 | 0.8717 | 77.05 | 0.8202 | - |
| Thepade *et al*. [8] | 6 | MLP | 0.5849 | 0.8264 | 0.5170 | 0.8868 | 0.5490 | 0.4310 |
| Bakheet *et al*. [16] | - | LDCRFs | 0.9617 | 0.9588 | 0.9446 | - | 0.9579 | - |
| Konar *et al*. [17] | - | CNN | 0.8900 | 0.9310 | 0.8350 | - | 0.8260 | - |
| Panwar *et al*. [18] | - | nCOVnet | 0.9762 | 0.8810 | 0.8200 | - | 0.8913 | - |
| Shukla *et al*. [19] | - | SVM | 0.9243 | 0.8779 | 0.9016 | - | 0.9128 | - |
| Echtioui *et al*. [20] | - | SVM | 0.9600 | 0.9414 | 0.8600 | - | 0.9107 | - |
| Podder *et al*. [21] | 111 | RF | 0.9400 | 0.9400 | 0.9400 | - | 0.9400 | - |
| **Our proposed method** | **22** | **KNN** | **1.0000** | **0.9996** | **0.9994** | **1.000** | **0.999** | **0.999** |
| **Our proposed method** | **22** | **SVM** | **0.9894** | **0.9737** | **0.9712** | **0.978** | **0.980** | **0.941** |

Based on the experimental results presented in Table 4, it can be concluded that the proposed method has a positive impact on the performance and exceeded the other state-of-the-art methods in terms of PRE, ACC, SEN, SP, F1, and MCC. On the other hand, the proposed method with the KNN classifier was sufficient to score the maximal PRE, ACC, SEN, SP, F1, and MCC performance among the remaining classifiers.

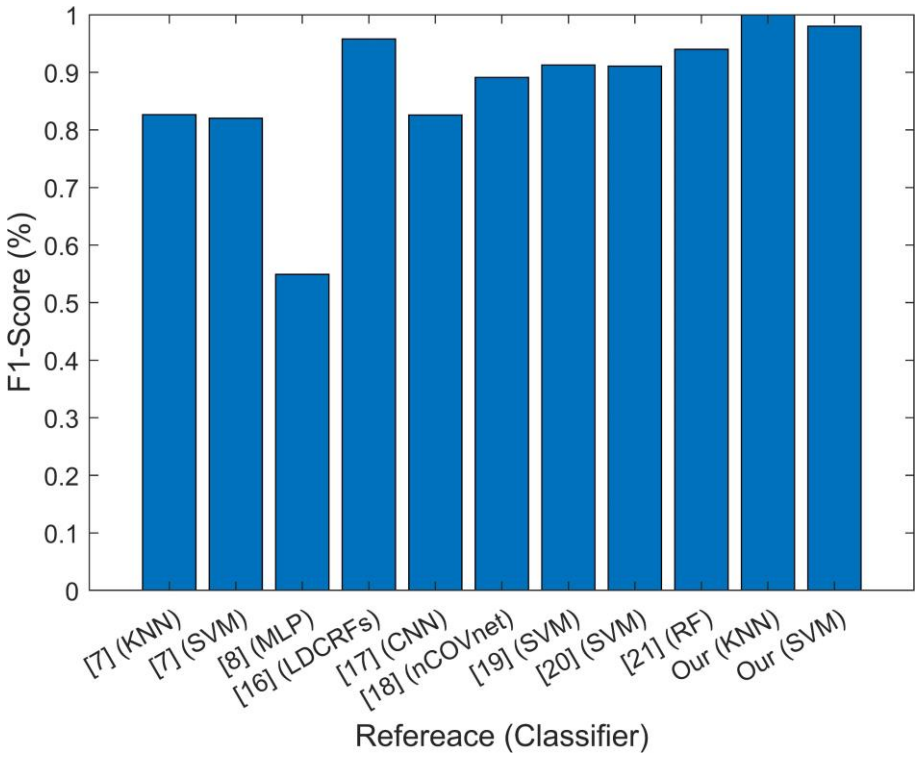


**Figure 6**. Comparison of accuracies for different classifiers

A similar fact has been concluded from Figure 6. The proposed method with the KNN and SVM classifiers, 0.9991 and 0.9416, respectively, was sufficient to score and achieve the highest F1-score performance among the remaining classifiers.

## Conclusions

This paper presents the GLCM with twenty-two features and machine learning classifiers to classify COVID-19 infection on chest X-ray images. In addition, x-ray images from the COVID-19 Radiography Database were used to test the proposed method's efficacy. Only 2399 chest X-ray images were chosen randomly: 1577 NORMAL and 822 COVID-19 from the COVID-19 Radiography Database. Twenty-two statistical texture features are extracted from each image using the GLCM analysis method. The proposed technique generates five GLCM matrixes. Two machine learning classifiers, KNN and SVM, are also trained using the extracted features from the GLCM matrices. Finally, the proposed method is compared to a current state-of-the-art approach. SEN, ACC, PRE, F1, SP, and MCC performances are all significantly improved by the proposed method, which is computationally efficient. In the future, we will try to use the entire COVID-19 Radiography Database to analyze the proposed method.

## Conflicts of Interest

The author(s) declare(s) that there is no conflict of interest regarding the publication of this paper.

## Acknowledgment

This work is part of a research project, FRGS19-090-0699, supported by the Ministry of Higher Education, Malaysia and University Technology of Malaysia.

## References

[1] WHO. (2020). WHO Director-General's opening remarks at the media briefing on COVID-19 - 11 March 2020. [Online]. Available: https://www.who.int/director-general/speeches/detail/who-director-general-s-opening-remarks-at-the-media-briefing-on-covid-19-11-march-2020.

[2] W. H. Organization. (2020). Coronavirus disease 2019 (COVID-19) situation report-51.

[3] Salim, A. A., Ghoshal, S. K., Suan, L. P., Bidin, N., Hamzah, K., Duralim, M., & Bakhtiar, H. (2018). Liquid media regulated growth of cinnamon nanoparticles: Absorption and emission traits. *Malaysian Journal of Fundamental and Applied Sciences*, *14*(3-1), 447-449.

[4] Hathot, S. F., Abbas, S. I., AlOgaili, H. A. T., & Salim, A. A. (2022). Influence of deposition time on absorption and electrical characteristics of ZnS thin films. *Optik*, *260*, 169056.

[5] Keni, R., Alexander, A., Nayak, P. G., Mudgal, J., & Nandakumar, K. (2020). COVID-19: emergence, spread, possible treatments, and global burden. *Frontiers in Public Health*, *216*.

[6] Vandenberg, O., Martiny, D., Rochas, O., van Belkum, A., & Kozlakidis, Z. (2021). Considerations for diagnostic COVID-19 tests. *Nature Reviews Microbiology*, *19*(3), 171-183.

[7] Salim, A. A., Bakhtiar, H., Ghoshal, S. K., & Huyop, F. (2020). Customised structural, optical and antibacterial characteristics of cinnamon nanoclusters produced inside organic solvent using 532 nm Q-switched Nd: YAG-pulse laser ablation. *Optics & Laser Technology*, *130*, 106331.

[8] Haralick, R. M., Shanmugam, K., & Dinstein, I. H. (1973). Textural features for image classification. *IEEE Transactions on Systems, Man, and Cybernetics*, *6*, 610-621.

[9] Singh, S., Srivastava, D., & Agarwal, S. (2017, August). GLCM and its application in pattern recognition. *2017 5th International Symposium on Computational and Business Intelligence (ISCBI)* (pp. 20-25). IEEE.

[10] Khudhair, K. T., Kadhim, O. N., Najjar, F. H., Abedi, F., Jamaluddin, A. N., & Al-Kharsan, I. H. (2022, May). Soft edge detection by mamdani fuzzy inference of color image. *2022 5th International Conference on Engineering Technology and its Applications (IICETA)* (pp. 379-383). IEEE.

[11] Salim, A. A., Ghoshal, S. K., Bakhtiar, H., Krishnan, G., & Sapingi, H. H. J. (2020, April). Pulse laser ablated growth of Au-Ag nanocolloids: Basic insight on physiochemical attributes. *Journal of Physics: Conference Series*.*1484*(1), 012011. IOP Publishing.

[12] Goyal, S., & Singh, R. (2021). Detection and classification of lung diseases for pneumonia and Covid-19 using machine and deep learning techniques. *Journal of Ambient Intelligence and Humanized Computing*, 1-21.

[13] Thepade, S. D., & Jha, H. (2021). COVID-19 identification using machine learning classifiers with GLCM features of chest x-ray images. *Trends in Sciences*, *18*(23), 46-46.

[14] Najjar, F. H., Al-Jawahry, H. M., Al-Khaffaf, M. S., & Al-Hasani, A. T. (2021, April). A novel hybrid feature extraction method using LTP, TFCM, and GLCM. *Journal of Physics: Conference Series*, *1892*(1), 012018.

IOP Publishing.
[15] Zhang, W., Pogorelsky, B., Loveland, M., & Wolf, T. (2021). Classification of COVID-19 X-ray images using a combination of deep and handcrafted features. *arXiv preprint arXiv*:2101.07866.
[16] Abbood, E. A., & Al-Assadi, T. A. (2022). GLCMs Based multi-inputs 1D CNN deep learning neural network for COVID-19 texture feature extraction and classification. *Karbala Int. J. Mod. Sci*., *8*(1), 28-39.
[17] Shaban, W. M., Rabie, A. H., Saleh, A. I., & Abo-Elsoud, M. A. (2020). A new COVID-19 patients detection strategy (CPDS) based on hybrid feature selection and enhanced KNN classifier. *Knowledge-Based Systems*, *205*, 106270.
[18] Ozdemir, M. A., Ozdemir, G. D., & Guren, O. (2021). Classification of COVID-19 electrocardiograms by using hexaxial feature mapping and deep learning. *BMC Medical Informatics and Decision Making*, *21*(1), 1-20.
[19] Shiri, I., Mostafaei, S., Haddadi Avval, A., Salimi, Y., Sanaat, A., Akhavanallaf, A., ... & Zaidi, H. (2022). High-dimensional multinomial multiclass severity scoring of COVID-19 pneumonia using CT radiomics features and machine learning algorithms. *Scientific Reports*, *12*(1), 14817.
[20] Chicco, D., & Jurman, G. (2020). The advantages of the Matthews correlation coefficient (MCC) over F1 score and accuracy in binary classification evaluation. *BMC Genomics*, *21*, 1-13.
[21] Bakheet, S., & Al-Hamadi, A. (2021). Automatic detection of COVID-19 using pruned GLCM-Based texture features and LDCRF classification. *Computers in Biology and Medicine*, *137*, 104781.
[22] Konar, D., Panigrahi, B. K., Bhattacharyya, S., Dey, N., & Jiang, R. (2021). Auto-diagnosis of COVID-19 using lung CT images with semi-supervised shallow learning network. *IEEE Access*, *9*, 28716-28728.
[23] Panwar, H., Gupta, P. K., Siddiqui, M. K., Morales-Menendez, R., & Singh, V. (2020). Application of deep learning for fast detection of COVID-19 in X-Rays using nCOVnet. *Chaos, Solitons & Fractals*, *138*, 109944.
[24] Waheed, S. R., Rahim, M. S. M., Suaib, N. M., & Salim, A. A. (2023). CNN deep learning-based image to vector depiction. *Multimedia Tools and Applications*, 1-20.
[25] Hathot, S. F., Jubier, N. J., Hassani, R. H., & Salim, A. A. (2021). Physical and elastic properties of $TeO_2$-$Gd_2O_3$ glasses: Role of zinc oxide contents variation. *Optik*, *247*, 167941.
[26] Salim, A. A., Ghoshal, S. K., & Bakhtiar, H. (2021). Growth mechanism and optical characteristics of Nd: YAG laser ablated amorphous cinnamon nanoparticles produced in ethanol: Influence of accumulative pulse irradiation time variation. *Photonics and Nanostructures-Fundamentals and Applications*, *43*, 100889.
[27] Shukla, P., Verma, A., Verma, S., & Kumar, M. (2020). Interpreting SVM for medical images using Quadtree. *Multimedia Tools and Applications*, *79*, 29353-29373.
[28] Ji, T., Liu, Z., Wang, G., Guo, X., Lai, C., Chen, H., ... & Zhou, Q. (2020). Detection of COVID-19: A review of the current literature and future perspectives. *Biosensors and Bioelectronics*, *166*, 11245.
[29] Salim, A. A., Ghoshal, S. K., Shamsudin, M. S., Rosli, M. I., Aziz, M. S., Harun, S. W., ... & Bakhtiar, H. (2021). Absorption, fluorescence and sensing quality of Rose Bengal dye-encapsulated cinnamon nanoparticles. *Sensors and Actuators A: Physical*, *332*, 113055.
[30] Podder, P., Bharati, S., Mondal, M. R. H., & Kose, U. (2021). Application of machine learning for the diagnosis of COVID-19. *Data Science for COVID-19* (pp. 175-194). Academic Press.
[31] Najjar, F. H., Khudhair, K. T., Khaleq, A. H. A., Kadhim, O. N., Abedi, F., & Al-Kharsan, I. H. (2022, May). Histogram features extraction for edge detection approach. *2022 5th International Conference on Engineering Technology and its Applications (IICETA)* (pp. 373-378). IEEE.
[32] Salim, A. A., Bakhtiar, H., Shamsudin, M. S., Aziz, M. S., Johari, A. R., & Ghoshal, S. K. (2022). Performance evaluation of rose bengal dye-decorated plasmonic gold nanoparticles-coated fiber-optic humidity sensor: A mechanism for improved sensing. *Sensors and Actuators A: Physical*, *347*, 113943.
[33] Ali, A. H., & Najjar, F. H. (2018, September). Integrating the kernel method to autonomous learning multi-model systems for online data. *2018 International Conference on Artificial Intelligence and Data Processing (IDAP)* (pp. 1-5). IEEE.